Am J Cancer Res 2026;16(10):4237-4253
www.ajcr.us /ISSN:2156-6976/ajcr0175589

Original Article

Remodeling of the tumor immune microenvironment and underlying oncogenic molecular mechanisms in HPV-associated OSCC

Ting Liu[1*], Changhuan Liu[2*], Xiaoyan Liu[3*], Ming Yu[4], Wenlong Wang[4], Xiangrui Ma[4,5], Yuanchen Wang[7], Jing Wang[6], Fang Wang[4], Tian Tian[7]

[1]Department of Orthodontics, Shandong Medical and Pharmaceutical University Hospital, Binzhou 256603, Shandong, China; [2]Department of Periodontal and Oral Mucosal Disease, Shenzhen Stomatology Hospital (Pingshan) of Southern Medical University, Shenzhen 518000, Guangdong, China; [3]Qilu Medical University, Zibo 255300, Shandong, China; [4]Department of Oral and Maxillofacial Surgery, Shandong Medical and Pharmaceutical University Hospital, Binzhou 256603, Shandong, China; [5]Department of Oral and Maxillofacial Surgery, West China Hospital of Stomatology, Sichuan University, Chengdu 610041, Sichuan, China; [6]Department of Endodontics, Shandong Medical and Pharmaceutical University Hospital, Binzhou 256603, Shandong, China; [7]Department of Periodontics, Shandong Medical and Pharmaceutical University Hospital, Binzhou 256603, Shandong, China. [*]Equal contributors and co-first authors.

Received July 23, 2026; Accepted September 24, 2026; Epub October 15, 2026; Published October 30, 2026

Abstract: Human papillomavirus (HPV)-positive oral squamous cell carcinoma (OSCC) possesses unique clinical and biological characteristics, while its specific clinicopathological features and underlying immune-molecular mechanisms remain unclear. This study aimed to systematically characterize the clinicopathological traits of HPV-associated OSCC and elucidate the key molecular and immune regulatory axes driving its malignant progression. We retrospectively analyzed the correlations between HPV infection status and multiple clinical parameters including age, gender, primary tumor location, clinical stage, pathological grade, and 5-year overall survival (OS) in OSCC patients. IHC was performed to detect the protein expression levels of p53, Cyclin D1 and pRb in OSCC tumor tissues, while flow cytometry was used to quantify the infiltration levels of myeloid-derived suppressor cells (MDSCs) and regulatory T cells (Tregs) in paired tumor tissues and peripheral blood specimens. Integrated transcriptomic RNA sequencing, miRNA target prediction and bioinformatic analyses were further conducted to screen core oncogenic immune targets and specific regulatory pathways in HPV-positive OSCC. Significant differences in primary tumor site, pathological differentiation and 5-year OS were identified between HPV-positive and HPV-negative OSCC patients, with no notable differences in age, gender and clinical stage across groups. And HPV-positive OSCC tissues presented markedly downregulated p53 and Cyclin D1 expression compared with the HPV-negative counterpart. MDSC levels progressively increased from controls to patients with oral precancerous lesions and OSCC, whereas Treg levels were significantly elevated in OSCC patients compared with both controls and patients with precancerous lesions. Bioinformatic analysis revealed that Calsequestrin 2 (CASQ2) expression was negatively correlated with tumor purity in HPV-positive OSCC, and two core circRNA-miRNA regulatory axes (hsa_circ_0058495/hsa-miR-2115-5p and hsa_circ_0032029/hsa-miR-2115-5p) were identified to target CASQ2 specifically. Collectively, HPV infection remodels the OSCC tumor microenvironment into an immunosuppressive phenotype via inducing abnormal accumulation of MDSCs and Tregs, thereby promoting OSCC malignant progression. The miRNA-mediated CASQ2 dysregulation may serve as a core pathogenic driver of HPV-positive OSCC. These findings uncover a novel immune-molecular mechanism underlying HPV-associated OSCC progression, and provide a theoretical basis for stratified precision immunotherapy for this unique OSCC subtype.

Keywords: Oral squamous cell carcinoma, human papillomavirus, tumor-associated myeloid-derived suppressor cells, regulatory T cells, Calsequestrin 2

Introduction

Oral squamous cell carcinoma (OSCC) represents the most prevalent malignant neoplasm of the maxillofacial region, accounting for over 90% of all malignancies arising at this anatomical site [1]. Statistics released by the Global Cancer Observatory indicate that more than

https://doi.org/10.62347/YYBR7909

300,000 new OSCC cases are diagnosed worldwide each year [2]. Over the past three decades, multimodal therapeutic strategies, including surgical resection, radiotherapy, and systemic chemotherapy, have undergone continuous technical refinement [3, 4]. Nevertheless, the 5-year overall survival (OS) rate for OSCC patients remains at approximately 50%. These marginal improvements in long-term prognosis, imposes a substantial burden on global public health systems [5, 6]. Accordingly, in-depth elucidation of the intrinsic pathological mechanisms governing OSCC initiation and progression, alongside identification of promising precision therapeutic targets, carries vital clinical implications and practical significance for optimizing patient survival outcomes.

Persistent infection with human papillomavirus (HPV) has been established as a novel independent risk factor for the initiation and progression of OSCC, in addition to tobacco and alcohol exposure [7]. The 8th edition staging manual of the American Joint Committee on Cancer clearly defines HPV-driven OSCC as a distinct disease subtype with exclusive pathogenic mechanisms and biological signatures [8]. Existing studies have validated that the high-risk HPV genome integrates into the genome of host epithelial cells and induces persistent expression of viral E6 and E7 oncoproteins. E6 mediates the degradation of tumor suppressor p53, while E7 disrupts cell cycle homeostasis. Collectively, they disrupt the physiological regulatory network of epithelial cell proliferation, endowing HPV-positive OSCC with poorly differentiated and non-keratinized pathological characteristics as well as enhanced invasive potential [9, 10]. Notably, large-cohort clinical investigations have uniformly demonstrated that, despite poorer tumor differentiation, HPV-positive OSCC possesses stronger tumor immunogenicity and higher responsiveness to radiotherapy, chemotherapy and immunotherapy [11, 12]. Patients with HPV-positive tumors experience reduced long-term risks of recurrence and distant metastasis, and consequently achieve favorable long-term survival [13]. In summary, HPV infection exerts a unique dual regulatory function during OSCC progression: it acts as a vital oncogenic driver initiating malignant transformation, and also serves as a specific biological indicator for predicting therapeutic response and clinical prognosis.

In recent years, the pivotal role of aberrant remodeling of the tumor immune microenvironment (TIME) in the malignant progression of OSCC has been progressively uncovered [14-16]. The TIME constitutes a dynamic, highly sophisticated microenvironmental system consisting of diverse innate and adaptive immune cell populations. Myeloid-derived suppressor cells (MDSCs) represent a heterogeneous subset of immature myeloid cells originating from the bone marrow. Previous studies have confirmed that the infiltration level of MDSCs is markedly higher in head and neck squamous cell carcinoma tissues than in mucosal atypical hyperplasia and normal oral mucosa [17]. Regulatory T cells (Tregs) are a specialized $CD4^+$ T cell subset uniquely characterized by the molecular marker FoxP3, which potently suppresses the activation, proliferation and anti-tumor effector functions of effector T cells [18]. To date, MDSCs and Tregs are widely recognized as two central pillars that facilitate tumor immune escape and establish an immunosuppressive microenvironment [19]. Although the pro-tumorigenic effects of these immunosuppressive cell populations have been preliminarily validated in head and neck malignancies, their distribution patterns, regulatory mechanisms and clinical implications in HPV-associated OSCC remain poorly defined, and the underlying molecular mechanisms require further systematic elucidation.

Calsequestrin 2 (CASQ2) is a high-capacity calcium-binding protein predominantly localized to the sarcoplasmic reticulum and endoplasmic reticulum, serving as a master regulator of calcium homeostasis [20]. Emerging evidence has identified CASQ2 as a novel tumor immunomodulator with great potential in reshaping the TIME. Nevertheless, its biological functions appear entirely divergent across distinct tumor types. In breast cancer, CASQ2 overexpression drives an aggressive malignant phenotype, facilitates the transformation of cancer-associated fibroblasts and collagen remodeling, and accelerates distant metastasis in vivo, indicative of its oncogenic role [21]. In stark contrast, studies using lung cancer models demonstrate that CASQ2 suppresses the JAK/STAT signaling cascade, reprograms tumor-associated macrophages from the pro-tumor M2 phenotype to the anti-tumor M1 phenotype, and consequently converts the immunosup-

pressive TIME into an anti-tumor immune-activated state, thereby exerting tumor-suppressive effects [22]. Such functional duality indicates that the immunomodulatory capacity of CASQ2 is highly context-dependent, governed by tumor origin and its unique microenvironment. To date, no published studies have characterized the expression profile and immunoregulatory functions of CASQ2 in OSCC, particularly HPV-positive OSCC, nor have they explored its potential crosstalk with the MDSC/Treg immune network.

In this study, we aimed to systematically explore the impacts of HPV infection on clinicopathological characteristics and prognosis among OSCC patients, and to elucidate the mechanisms by which HPV modulates the TIME via MDSC/Treg-mediated pathways. Additionally, we screened and validated CASQ2 as a core therapeutic target and further predicted its upstream regulatory signaling cascades. The results of this study will provide novel experimental evidence and promising therapeutic targets for stratified precise diagnosis and immunotherapy specific to HPV-positive OSCC.

Materials and methods

Case selection

Clinical pathological information was collected from OSCC patients admitted to West China Hospital of Stomatology, Sichuan University, and Shandong Medical and Pharmaceutical University Hospital, between January 1, 2013 to December 31, 2015 and January 1, 2018 to January 20, 2022. The collected information included age, sex, pathological grade, tumor site, and clinical stage. The cohort comprised 592 males and 288 females, with ages ranging from 16 to 89 years and a median age of 63 years. Patients who had received preoperative chemotherapy, hormone therapy, or radiotherapy were excluded from the study. In addition, a total of 200 tissue and peripheral blood samples from OSCC patients were collected prospectively during the last two years of the study period. OSCC tissues were obtained from surgically resected primary tumors, precancerous tissues were derived from surgical excisions or biopsies, and normal control tissues were harvested from margins adjacent to surgical incisions during procedures for oral cysts, benign tumors, or impacted teeth. Tissue specimens were placed in cryopreservation tubes within 15 min after surgical resection and immediately preserved in liquid nitrogen. Peripheral blood samples were processed within 2 h after collection, and cells were isolated for flow cytometric analysis. Each patient provided written informed consent for sample collection and subsequent experiments in accordance with ethical guidelines. This study was approved by the Ethics Committee of West China School of Stomatology, Sichuan University (approval No. WCHSIRB-D-2012-097), Ethics Committee of West China School of Stomatology, Sichuan University (approval No. WCHSIRB-D-2021-022), and Ethics Committee of Shandong Medical and Pharmaceutical University Hospital (approval No. 2017-015-01).

Immunohistochemistry (IHC)

Tissues were fixed in 4% neutral formaldehyde, dehydrated, embedded in paraffin. Sections (4 μm) were deparaffinized, rehydrated, and subjected to antigen retrieval in 0.01 M citrate buffer (pH 6.0) at 98°C for 15 min. After blocking with 3% H_2O_2 and 10% goat serum, sections were incubated overnight at 4°C with: anti-p16 (1:500, Santa Cruz, sc-56330), anti-p53 (1:500, Abcam, ab131442), anti-Cyclin D1 (1:500, Proteintech, 60186-1-Ig), anti-CASQ2 (1:500, HCUSABIO, CSB-PA004557LA01HU). Negative controls: PBS or isotype IgG; positive controls: known positive tissue sections. Secondary antibody (goat anti-mouse/rabbit IgG, Vector, PK-6100, 1:200) 30 min at room temperature, DAB 3-5 min, hematoxylin 1-3 min, dehydrated, mounted. Positivity: ≥10% cells with nuclear brown staining.

Flow cytometry

Peripheral blood (100 μL) diluted to 200 μL with PBS, stained with antibody cocktail: CD11b-PE-Cy7 (clone ICRF44, BioLegend 301-322), Lineage-FITC (CD3/CD14/CD16/CD19/CD20/CD56 cocktail, BD Biosciences), HLA-DR-APC (clone L243, BioLegend 307616), CD33-PE (clone WM53, BioLegend 303404). Incubate 4°C 30 min dark, RBC lysis, wash ×3 with PBS, fix with 0.1% formaldehyde, acquire on FC500 within 2 h. Gating: FSC/SSC exclude debris → doublet exclusion (FSC-H vs. FSC-A) → $CD11b^+$ LIN^- $HLA\text{-}DR^-$ $CD33^+$ for MDSC. Isotype or FMO controls were used for gate setting.

For tissue: mince, homogenize to single-cell suspension, wash with serum-free medium + 1% BSA, stain with same MDSC panel, incubate 30 min dark, wash twice with PBS + 1% BSA, acquire on FC500. For Treg: surface stain CD4-FITC (clone RPA-T4, BioLegend 300506) + CD25-PE (clone BC96, BioLegend 302604), then fix/permeabilize with FoxP3 Kit (eBioscience 00-5523-00), intracellular stain FoxP3-APC (clone 236A/E7, eBioscience 17-4777-42) 30 min 4°C dark, wash, acquire.

Real-time quantitative polymerase chain reaction (RT-qPCR) analysis

Total RNA from tissues was extracted using RNAex Pro Reagent (Accurate Biology, Changsha, China). Reverse transcription to cDNA was performed with the Evo M-MLV Reverse Transcription Kit (Accurate Biology, Changsha, China). RT-qPCR was performed using the SYBR Green PCR Kit (Accurate Biology, Changsha, China). The relative expression levels of genes were quantified using the $2^{-\Delta\Delta CT}$ method, and normalized with the GAPDH level. The specific primers used are as follows (**Table 8**).

Transcriptome sequencing analysis

The transcriptome sequencing data used in this study were from the previously self-sequenced dataset of our research group (PMID: 37664656), which included 3 HPV-positive and 3 HPV-negative oral squamous cell carcinoma tissue samples. Sequencing was performed using the Illumina NovaSeq 6000 platform (GPL24676), and the raw sequencing data along with the expression matrix have been uploaded to the NCBI GEO database (GSE190224). Differentially expressed genes were screened using the limma package in R software, with a screening threshold of $|log2FC| \geq 1$ and FDR <0.05. The differentially expressed genes were imported into the STRING database to construct a protein-protein interaction network, with an interaction confidence cutoff set at 0.4, and network visualization was performed using Cytoscape software. The TIMER database (http://timer.cistrome.org) was utilized to analyze the correlation between target gene expression and patient prognosis. Kaplan-Meier method was employed to plot survival curves, and the Cox proportional hazards regression model was used to evaluate the impact of gene expression levels on patient overall survival.

Statistical analysis

Statistical analyses were performed using SPSS software (version 25.0) and R software. Categorical variables were presented as frequencies and percentages, whereas continuous variables were expressed as the mean ± standard deviation (SD) or median with interquartile range [median (Q1-Q3), as appropriate. The normality of continuous variables was assessed using the Shapiro-Wilk test, and homogeneity of variance was evaluated using Levene's test.

The chi-square (χ^2) test or Fisher's exact test, as appropriate, was used to evaluate associations between categorical variables, including HPV infection status, clinicopathological characteristics, and the expression status of cell cycle-related proteins (p53, pRb, and Cyclin D1). Kaplan-Meier survival analysis was used to estimate 5-year OS, and differences between survival curves were assessed using the log-rank test.

For comparisons of continuous variables among the control, precancerous lesion, and OSCC groups, one-way analysis of variance (ANOVA) was used when the assumptions of normality and homogeneity of variance were satisfied; otherwise, the Kruskal-Wallis test was applied. When the overall test indicated a statistically significant difference, appropriate post hoc pairwise comparisons were subsequently performed. For nonparametric analyses, Dunn's post hoc test was used, with *P* values adjusted using the Benjamini-Hochberg false discovery rate (FDR) procedure to account for multiple comparisons. Effect sizes were additionally calculated to quantify the magnitude of between-group differences. All statistical tests were two-sided, and P<0.05 was considered statistically significant.

Results

Relationship between HPV infection status and clinicopathological characteristics in OSCC patients

The relationship between HPV infection status and clinicopathological characteristics in OSCC patients was presented in **Table 1**. A significant association was observed between HPV infection status and tumor site. The proportions of HPV-positive OSCC cases at differ-

Table 1. Relationship between HPV infection and clinicopathological indicators in patients with OSCC

Clinical pathological indicators	HPV		*P*-value
	(+)	(-)	
Age			0.2194
<60	117	402	
≥60	69	292	
Gender			0.8426
Male	124	468	
Female	62	226	
Tumor location			<0.0001
Gingiva	14	67	
Tongue	65	237	
Palate	8	40	
Cheek	39	209	
Floor of mouth	20	87	
Lip	5	14	
Pterygomandibular raphe area	2	3	
Pharynx	33	37	
Clinical staging			0.1527
I	36	106	
II	41	141	
III	43	138	
IV	66	309	
Pathologic grading			<0.0001
I	64	341	
II	60	223	
III	62	130	
Postoperative recurrence, metastasis or death			0.7704
Yes	8	27	
No	53	203	

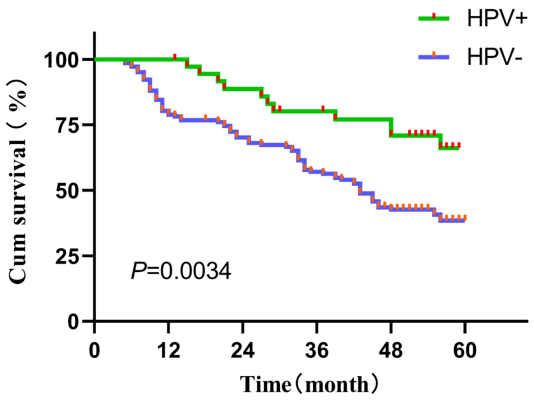

Figure 1. HPV infection status and 5-year OS in patients with OSCC.

ent sites were as follows: gingiva, 7.53%; tongue, 34.94%; palate, 4.30%; buccal mucosa, 20.97%; floor of mouth, 10.75%; lip, 2.69%; pterygomandibular raphe area, 1.08%; and oropharynx, 17.74%. Differences in HPV infection status among tumor sites were statistically significant (P<0.0001), indicating a correlation between HPV infection status and tumor location in OSCC.

Furthermore, HPV infection status differed significantly across pathological grades. The proportions of HPV-positive cases were 34.41% in Grade I, 32.26% in Grade II, and 33.33% in Grade III OSCC specimens. This stepwise increase in HPV prevalence with advancing tumor grade was statistically significant (P<0.0001), indicating a positive association between HPV positivity and higher pathological grade in OSCC.

No statistically significant associations were found between HPV infection status and age, sex, or clinical stage as defined by the AJCC 8th edition (P = 0.2194, 0.8426, and 0.1527, respectively). Likewise, HPV status showed no significant correlation with postoperative disease progression-defined as recurrence, metastasis, or death (P = 0.7704). Collectively, these findings suggest that in this OSCC cohort, HPV infection status is independent of age, sex, clinical stage, and post-treatment outcomes.

Relationship between HPV infection status and 5-year OS in OSCC patients

Patients who completed 5 years of postoperative follow-up were selected from the cohort of 880 patients to analyze the relationship between HPV infection status and 5-year OS (**Figure 1**). Statistical analysis revealed that the 5-year OS rate of HPV-positive OSCC patients was significantly higher than that of HPV-negative OSCC patients (P = 0.0034).

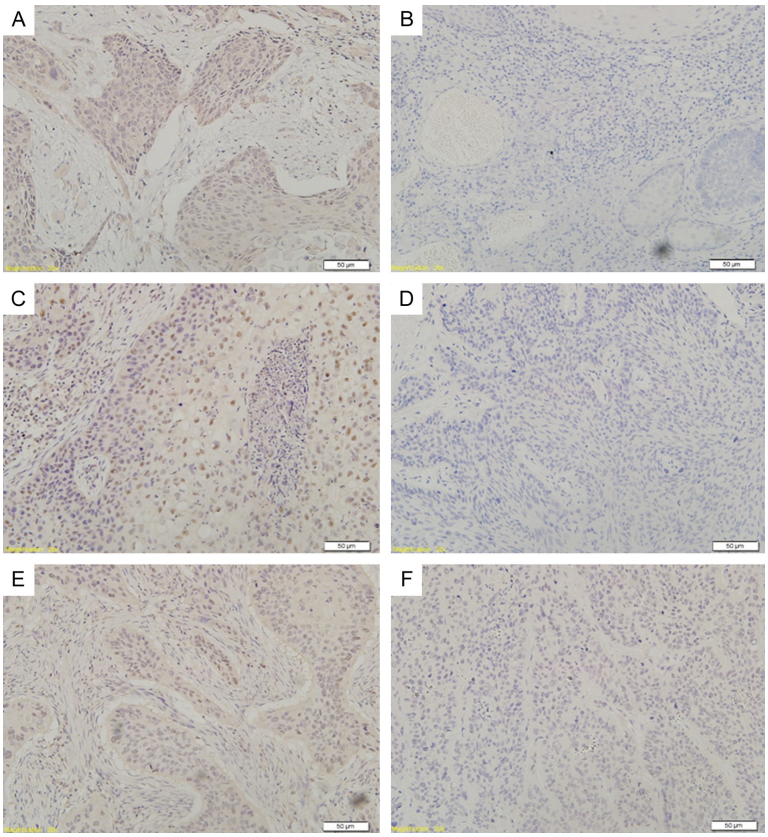

Figure 2. IHC staining of p53, Cyclin D1 and pRb in OSCC tissues (200×). A. p53 positive. B. p53 negative. C. Cyclin D1 positive. D. Cyclin D1 negative. E. pRb positive. F. pRb negative.

Table 2. Protein expression of cyclins relative to HPV infection status in OSCC

Cell cycle-related proteins	HPV		*P*-value
	(+)	(-)	
P53			0.0006
(+)	50	228	
(-)	61	131	
pRb			0.535
(+)	6	7	
(-)	12	9	
Cyclin D1			0.0155
(+)	25	143	
(-)	66	203	

Molecular pathological correlates of HPV infection: p53, Cyclin D1, and pRb expression

To elucidate the molecular pathological landscape associated with HPV infection in OSCC, we evaluated the expression of p53, Cyclin D1, and pRb, which were presented in **Figure 2**. The results demonstrated that HPV infection status in OSCC was significantly associated with their expression (**Table 2**). Among HPV-positive OSCC cases, 45.05% were p53-positive and 54.95% were p53-negative. Statistical analysis indicated a significant association between p53 expression and HPV infection status in OSCC patients (P = 0.0006). Similarly, cyclin D1 positivity was detected in 27.47% of HPV-positive OSCC tissues, while 72.53% exhibited negative staining. Statistical analysis further confirmed that Cyclin D1 expression differed significantly between HPV-positive and HPV-negative OSCC patients (P = 0.0155). However, no statistically significant difference was observed in pRb expression levels between HPV-positive and HPV-negative OSCC patients (P = 0.535).

Relationship between the change of TIME and HPV infection status in OSCC patients

The role of the TIME in OSCC progression has attracted increasing attention. Accordingly, we further evaluated MDSC and Treg levels in peripheral blood and tissue samples from the control, precancerous lesion, and OSCC groups (**Figures 3**-**6**). Prior to intergroup comparisons, the distribution and homogeneity of variance of MDSC and Treg data were assessed using the Shapiro-Wilk and Levenend tests, respectively. The normality analysis showed that all blood and tissue MDSC measurements deviated significantly from a normal distribution (all P<0.05; Table S1). For Tregs, non-normal distributions were observed for blood Tregs in the control group and tissue Tregs in the OSCC group, whereas the remaining groups showed no significant deviation from normality (Table S2). Leveneen test further demonstrated significant heterogeneity of variance for both MDSC and

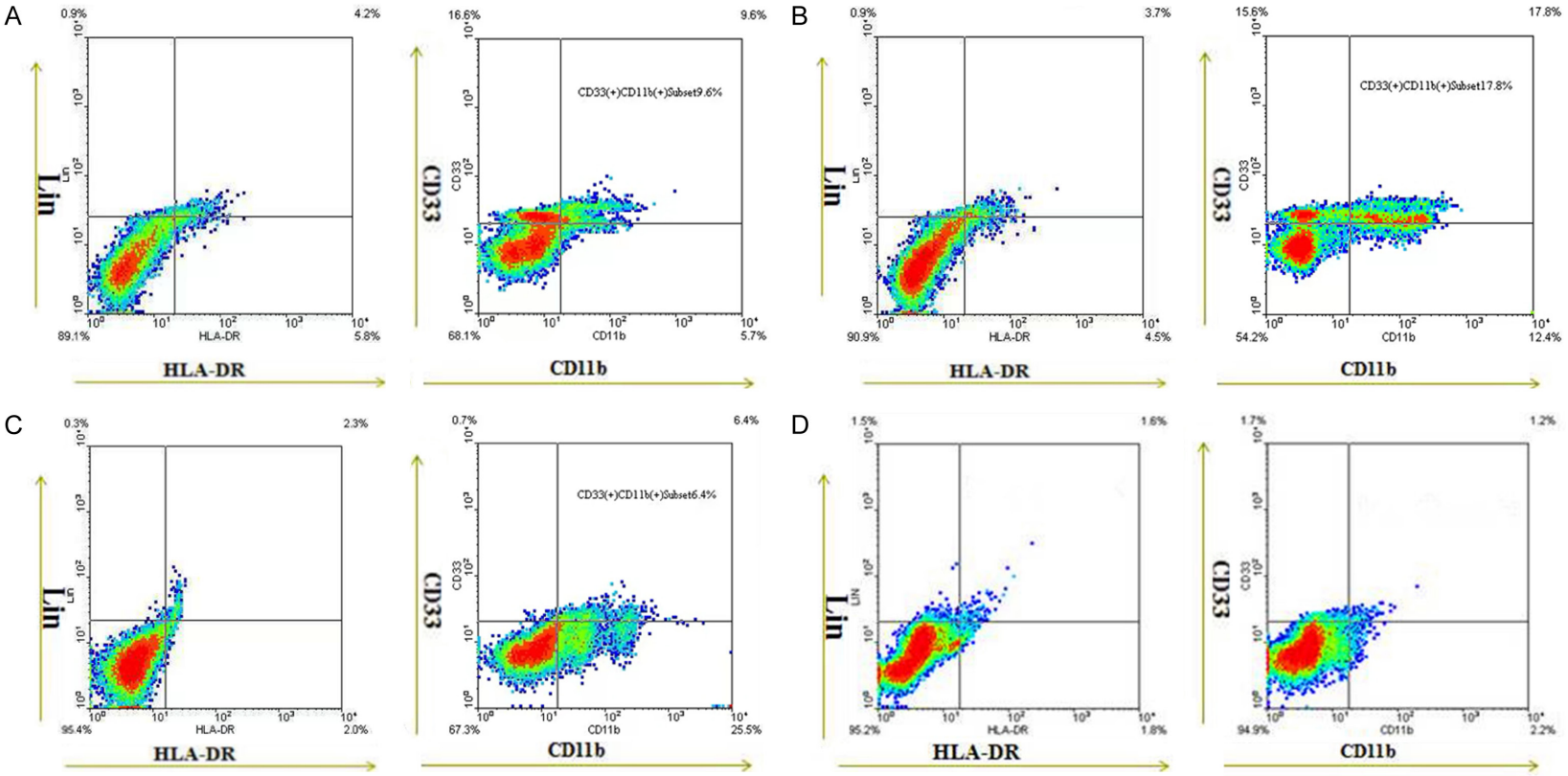

Figure 3. MDSC positive rates in the peripheral blood of patients with different oral lesions. A. The representative flow cytometry dot plot of MDSCs in the peripheral blood of HPV-negative OSCC patients. B. The representative flow cytometry dot plot of MDSCs in the peripheral blood of HPV-positive OSCC patients. C. The representative flow cytometry dot plot of MDSCs in the peripheral blood of precancerous lesions patients. D. The representative flow cytometry dot plot of MDSCs in the peripheral blood of healthy individuals.

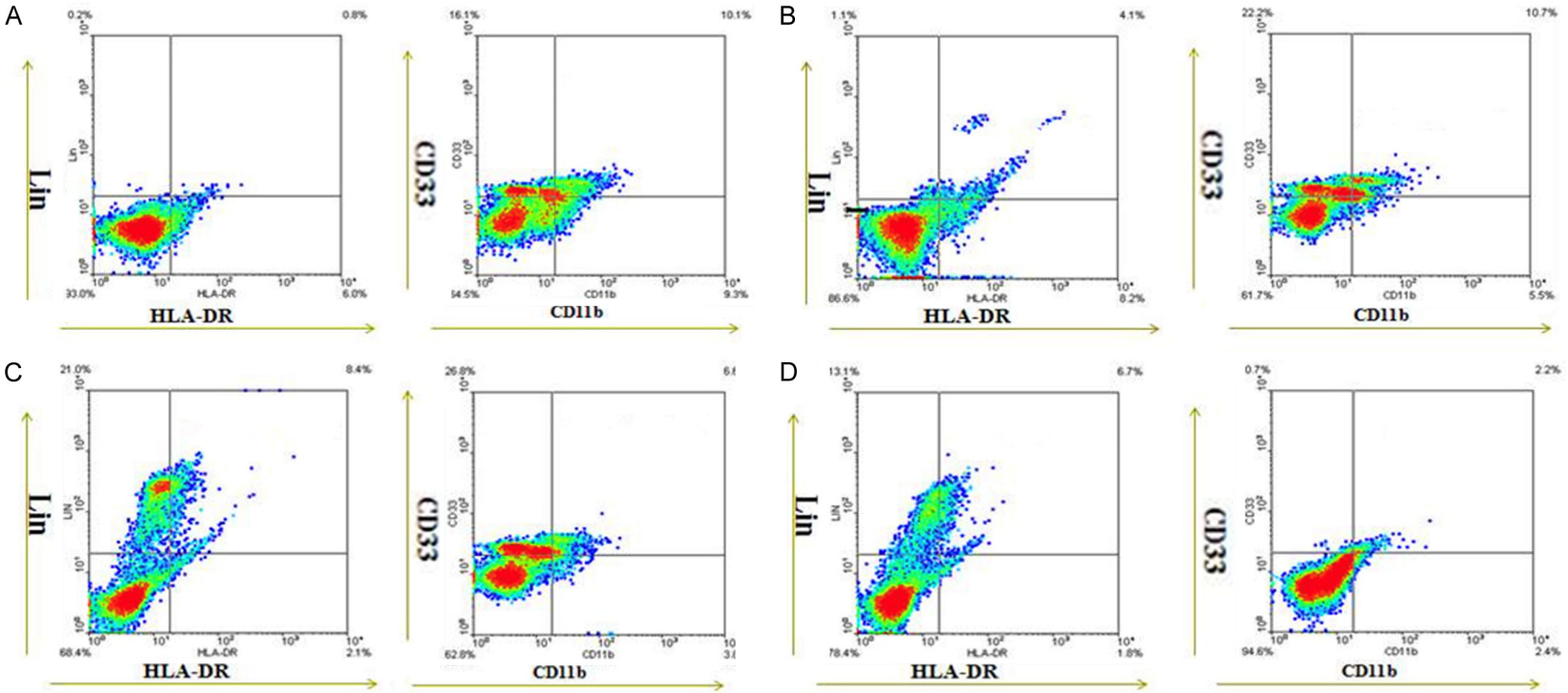

Figure 4. MDSC positive rates in tissues of the OSCC, precancerous lesion and control groups. A. The representative flowcytometry dot plot of MDSCs in the tissue of HPV-negative OSCC patients. B. The representative flowcytometry dot plot of MDSCs in the tissue of HPV-positive OSCC patients. C. The representative flowcytometry dot plot of MDSCs in the tissue of precancerous lesions patients. D. The representative flowcytometry dot plot of MDSCs in the tissue of healthy individuals.

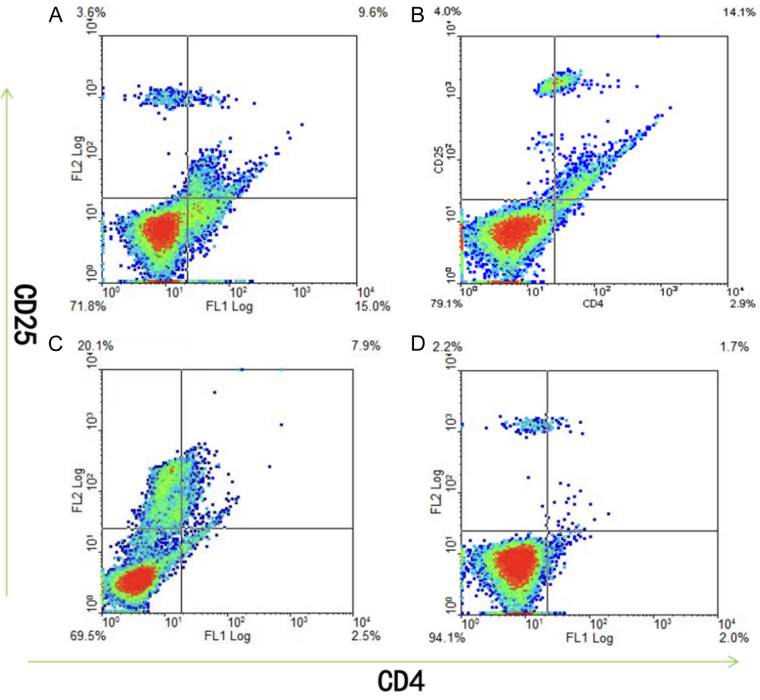

Figure 5. Treg positive rates in the peripheral blood of patients with different oral lesions. A. The representative flow cytometry dot plot of Tregs in the peripheral blood of HPV-negative OSCC patients. B. The representative flow cytometry dot plot of Tregs in the peripheral blood of HPV-positive OSCC patients. C. The representative flow cytometry dot plot of Tregs in the peripheral blood of precancerous lesions patients. D. The representative flow cytometry dot plot of Tregs in the peripheral blood of healthy individuals.

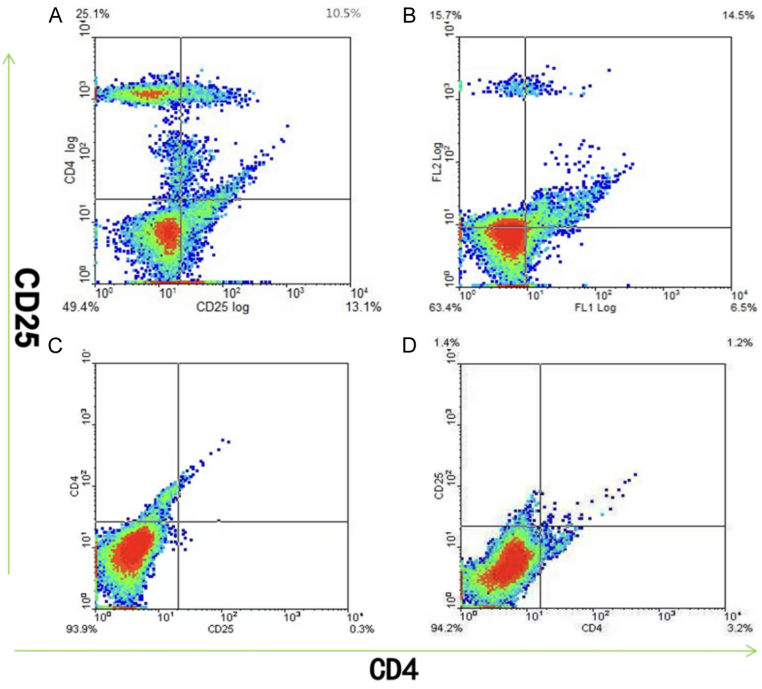

Figure 6. Treg positive rates in tissues of the OSCC, precancerous lesion and control groups. A. The representative flow cytometry dot plot of Treg in the tissue of HPV-negative OSCC patients. B. The representative flow cytometry dot plot of Treg in the tissue of HPV-positive OSCC patients. C. The representative flow cytometry dot plot of Treg in the tissue of precancerous lesions patients. D. The representative flow cytometry dot plot of Treg in the tissue of healthy individuals.

Treg measurements in peripheral blood and tissue samples (all $P<0.05$; Tables S3 and S4). Accordingly, the Kruskal-Wallis test was used for the overall comparisons among the three groups. Significant overall differences in MDSC levels were observed among the control, precancerous lesion, and OSCC groups in both peripheral blood and tissue samples (both $P<0.001$; **Table 3**). Subsequent Dunned for the overall comparisons among the three groups. Significant overall differences in MDSC levels were observed and tissue MDSCs (all FDR-adjusted $P<0.05$; Table S5), with MDSC levels progressively increasing from the control group to the precancerous lesion group and then to the OSCC group.

Similarly, significant overall differences in Treg levels were observed among the three groups in both peripheral blood and tissue samples (both $P<0.001$; **Table 4**). Dunn were observed among the three grTreg levels in the OSCC group were significantly higher than those in both the control and precancerous lesion groups (all FDR-adjusted $P<0.001$; Table S6). In contrast, no significant differences were observed between the control and precancerous lesion groups for either blood or tissue Treg levels (FDR-adjusted

Table 3. The level of MDSCs in OSCC group, precancerous lesion group and control group

Variable	Control (n = 30)	Precancerous lesion (n = 30)	OSCC (n = 200)	Kruskal-Wallis H	df	*P* value	η^2(H)
Blood MDSC	0.580 (0.323-0.950)	3.875 (1.720-4.947)	7.650 (6.680-12.560)	116.396	2	<0.001	0.445 (large)
Tissue MDSC	0.585 (0.335-1.127)	4.345 (3.312-5.567)	9.910 (7.865-14.030)	128.663	2	<0.001	0.493 (large)

Note: Data are presented as median (Q1-Q3). Because the assumptions of normality and/or homogeneity of variance were not satisfied, overall differences among the three groups were assessed using the Kruskal-Wallis test. η^2(H) represents the Kruskal-Wallis effect size.

Table 4. The level of Tregs in OSCC group, precancerous lesion group and control group

Variable	Control (n = 30)	Precancerous lesion (n = 30)	OSCC (n = 200)	Kruskal-Wallis H	df	*P* value	η^2(H)
Blood Treg	0.730 (0.297-1.297)	1.860 (0.295-2.607)	10.395 (9.578-11.280)	138.178	2	<0.001	0.530 (large)
Tissue Treg	0.625 (0.448-0.838)	1.210 (0.405-1.595)	9.650 (8.300-11.067)	138.227	2	<0.001	0.530 (large)

Note: Data are presented as median (Q1-Q3). Because the assumptions of normality and/or homogeneity of variance were not satisfied, overall differences among the three groups were assessed using the Kruskal-Wallis test. η^2(H) represents the Kruskal-Wallis effect size.

Table 5. The level of MDSCs in HPV-positive group and HPV-negative group

Group	N	Peripheral blood	*P*-value	N	Tissue	*P*-value
HPV+	47	13.84%±1.96%	<0.0001	39	15.78%±2.84%	<0.0001
HPV-	153	9.14%±0.92%		161	8.45%±0.87%	

Table 6. The level of Tregs in HPV-positive group and HPV-negative group

Group	N	Peripheral blood	*P*-value	N	Tissue	*P*-value
HPV+	47	15.74±2.10%	<0.0001	39	14.73±1.76%	<0.0001
HPV-	153	9.62%±0.64%		161	8.77%±1.18%	

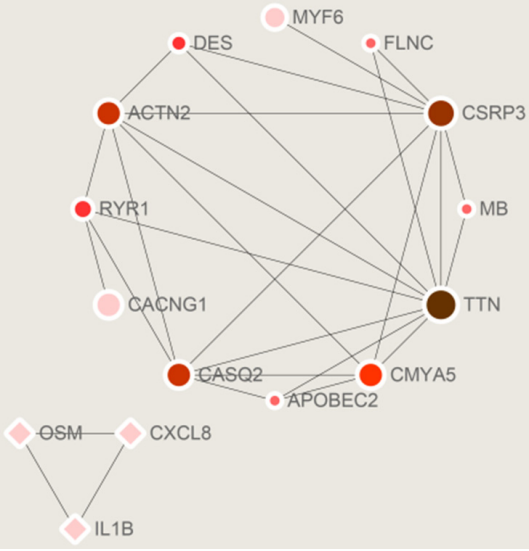

Figure 7. Network analysis of differential gene-protein interactions.

P = 0.622 and 0.589, respectively). Furthermore, when HPV-positive and HPV-negative OSCC patients were compared, the levels of MDSCs and Tregs in both peripheral blood and tissue samples were significantly higher in HPV-positive patients than in HPV-negative patients (P<0.0001). Detailed statistical analyses and comparisons are presented in **Tables 5** and **6**.

Prediction of potential prognostic targets using high-throughput sequencing data combined with immune-related databases

A co-expression confidence score threshold of 0.4 was applied using the STRING database. A total of 15 proteins were identified as exhibiting co-expression relationships (**Figure 7**). These molecules were ranked in descending order according to degree centrality values as follows: TTN, CSRP3, ACTN2, CASQ2, CMYA5, RYR1, APOBEC2, DES, CXCL8, FLNC, IL1B, MB, OSM, CACNG1, and MYF6. Among these molecules, CXCL8, IL1B, and OSM were highly expressed in OSCC samples, whereas RYR1, TTN, MYF6, MB, DES, CSRP3, FLNC, ACTN2, CACNG1, CASQ2, CMYA5, and APOBEC2 were expressed at low levels. Prognostic analysis

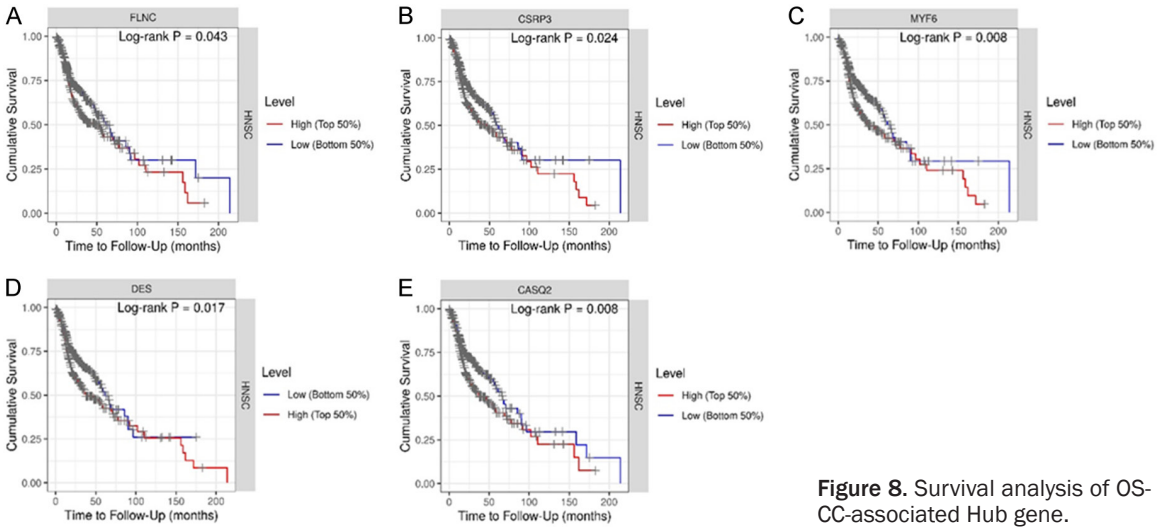

Figure 8. Survival analysis of OSCC-associated Hub gene.

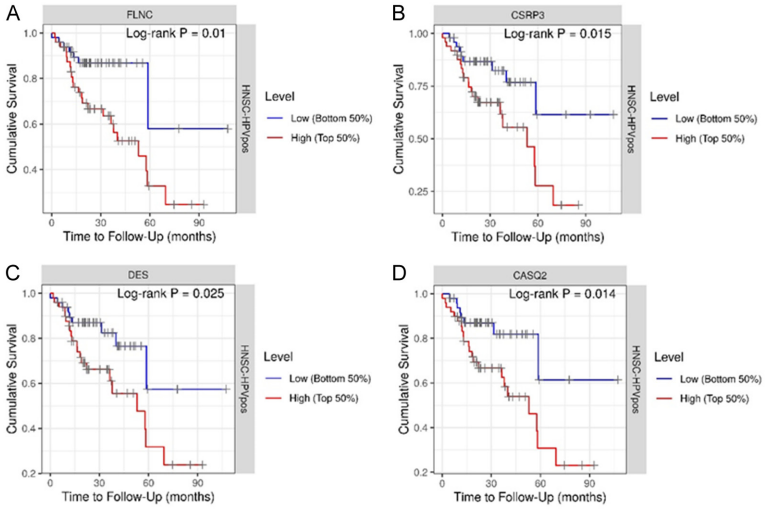

Figure 9. Survival analysis of hub genes associated with HPV-positive OSCC.

was conducted using the TIMER database. Low expression of FLNC, CSRP3, MYF6, DES, and CASQ2 was significantly associated with improved survival in OSCC patients (P<0.05) (**Figure 8**). Similarly, low expression of FLNC, CSRP3, DES, and CASQ2 was significantly associated with improved survival in HPV-positive OSCC patients (P<0.05) (**Figure 9**).

Pearson correlation analysis of tumor purity showed that, in the overall OSCC cohort, CASQ2 expression exhibited the strongest correlation with tumor purity, with a coefficient of r = -0.156; DES yielded a coefficient of r = -0.121, and both associations were statistically significant (P<0.05) (**Figure 10A**, **10D**). Stratified analyses further revealed that the correlation coefficients for CASQ2 and tumor purity were -0.224 in HPV-positive OSCC and -0.130 in HPV-negative OSCC, both of which were statistically significant (P<0.05) (**Figure 10B**, **10C**). For DES, significant correlation with tumor purity was observed only in the HPV-positive subgroup (r = -0.214, P<0.05), while no statistical significance was detected in HPV-negative OSCC (r = -0.082, P>0.05) (**Figure 10E**, **10F**). The results of RT-qPCR and IHC assays confirmed that CASQ2 was significantly downregulated in HPV-positive OSCC compared with HPV-negative OSCC (**Figure 11A**, **11B**). Collectively, these findings suggest that CASQ2 plays a more prominent regulatory role than DES in HPV-related OSCC.

Subsequently, we further predicted the upstream post-transcriptional regulatory network governing CASQ2 expression to explore its potential regulatory mechanisms in HPV-associated OSCC. We intersected the predicted miRNA target binding data with miRNA expression profiles obtained from matched tumor datasets. The candidate miRNAs were then subjected to intersection analysis with differentially expressed circular RNAs (circRNAs) detected by high-throughput sequencing (**Figure 12**), and circRNAs that co-expressed with the

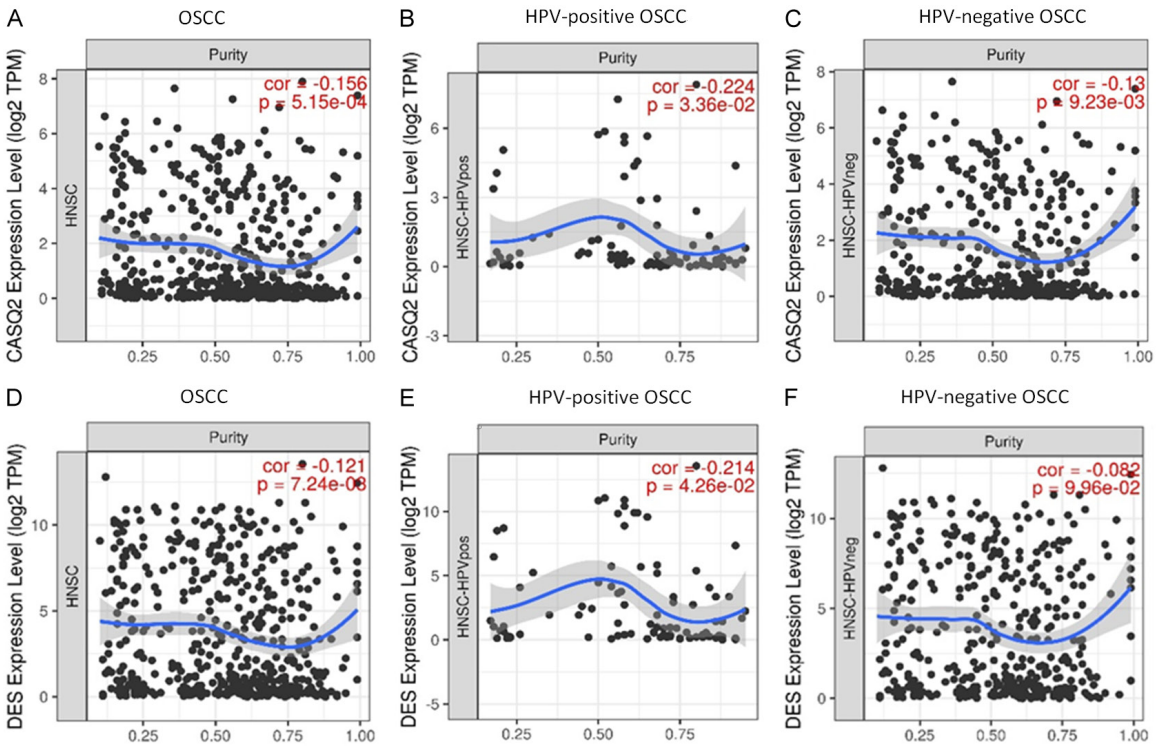

Figure 10. The tumor purity analysis of CASQ2.

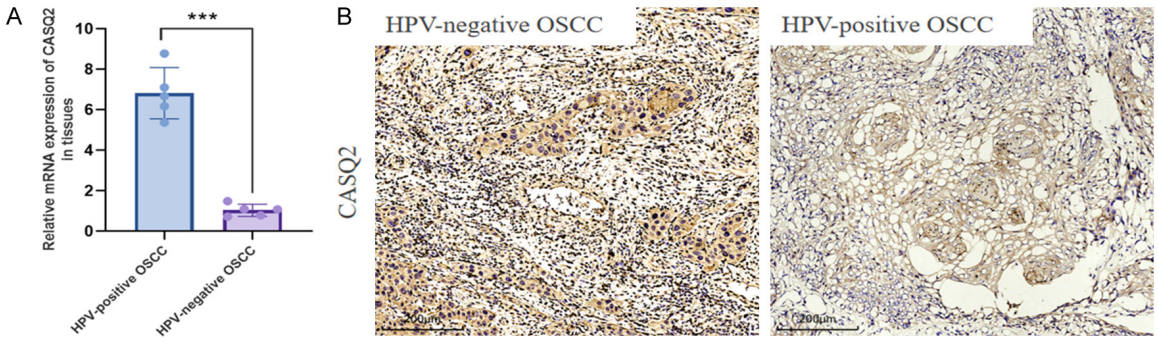

Figure 11. The expression levels of CASQ2 in tissues. A. The RT-qPCR analysis of CASQ2 in HPV-positive and HPV-negative OSCC tissues. B. Representative IHC images of CASQ2 in HPV-positive and HPV-negative OSCC tissues.

target mRNA CASQ2 and exhibited consistent expression trends were selected as candidate regulatory molecules. This multi-layered integrative analysis ultimately yielded five candidate circRNAs (**Table 7**) and identified two high-confidence regulatory axes: hsa_circ_0058495/hsa-miR-2115-5p/CASQ2 and hsa_circ_0032029/hsa-miR-2115-5p/CASQ2. These regulatory axes represent promising biological pathways that may shape the immunosuppressive tumor microenvironment during the initiation and progression of HPV-driven OSCC.

Discussion

This retrospective study enrolled a cohort of 880 patients diagnosed with OSCC to explore the correlations between HPV infection status and a full panel of clinicopathological indicators, as well as to evaluate the prognostic value of HPV positivity. Consistent with previous epidemiological and clinical reports, our analyses showed that HPV positivity in OSCC was significantly associated with tumor anatomical subsites and pathological differentiation grades. In contrast, no significant associations were ob-

Figure 12. Identification of the miRNA by Wenn analysis.

Table 7. Five circRNAs with differential expression

cirRNA	GCP_readcount	GCN_readcount	log2FoldChange	Regulation
hsa_circ_0001977	4.251961151	0	4.5828	Up
hsa_circ_0001236	7.804472456	0.780138649	2.943	Up
hsa_circ_ 0003118	4.457126887	0	4.6539	Up
hsa_circ_0058495	1.439266597	8.383997559	-2.8798	Down
hsa_circ_0032029	1.293719408	8.200062997	-2.4967	Down

Table 8. Primers for qRT-PCR

Gene	Forward	Reverse
CASQ2	CCTTGCCATCCCCAACAAACCT	CGACGTAGAGFGGGTCTTTGGT
GAPDH	GGAAGCTTGTCATCAATGGAAATC	TGATGACCCTTTTGGCTCCC

served between HPV status and patient age, sex, clinical tumor stage, or short-term postoperative disease progression [23, 24]. The elevated HPV-positive rate observed in oropharyngeal lesions within our cohort recapitulates this inherent viral tissue preference and validates the anatomical distribution patterns documented in large-scale multicenter clinical cohorts [25].

Regarding the correlation between HPV status and pathological differentiation, HPV positivity was closely linked to poorly differentiated tumor histology, yet patients with HPV-positive OSCC achieved markedly superior 5-year OS. This seemingly contradictory observation aligns with the prevailing consensus in the field: histological grade alone cannot reliably predict prognosis in HPV-associated malignancies. Instead, intrinsic tumor molecular signatures and the TIME serve as the primary determinants of clinical outcomes [26]. In our cohort, HPV infection status bore no statistically significant correlation with clinical tumor stage (P = 0.1527), postoperative recurrence, distant metastasis, or tumor-specific mortality (P = 0.7704). This inconsistency with prior studies focused solely on oropharyngeal carcinoma may stem from the greater etiological heterogeneity of oral cavity OSCC. Concurrent tobacco and alcohol exposure reshapes the distribution of clinical stages and attenuates stage-based disparities in HPV prevalence across patient subgroups [27, 28].

IHC detection demonstrated significantly lower expression of p53 and Cyclin D1 in HPV-positive OSCC specimens, while pRb expression levels were comparable between HPV-positive and HPV-negative groups (P = 0.535). Kaplan-Meier survival analysis coupled with log-rank testing demonstrated that patients with HPV-positive OSCC exhibited significantly prolonged 5-year OS relative to HPV-negative counterparts (P = 0.0034). This result corroborates and extends existing literature identifying HPV positivity as a favorable prognostic biomarker for head and neck squamous cell carcinoma (HNSCC). HPV-associated OSCC exhibits unique oncogenic

signaling programs and therapeutic responsiveness that collectively confer a survival advantage, driven by multi-layered molecular and immunological mechanisms. At the molecular level, HPV-positive tumors carry no oncogenic TP53 missense mutations; cytotoxic DNA-damaging therapies such as cisplatin and radiotherapy can restore wild-type p53 function and enhance tumor treatment sensitivity [29]. Immunologically, HPV-positive tumor cells express viral neoantigens encoded by the E6 and E7 oncoproteins, rendering lesions highly immunogenic and susceptible to sustained adaptive immune surveillance. In line with this mechanism, abundant intratumoral infiltration of $CD8^+$ cytotoxic T lymphocytes is frequently detected in HPV-driven HNSCC [30].

Flow cytometric immunophenotyping revealed that the proportions of MDSCs and Tregs in paired peripheral blood and tumor tissue samples were significantly higher in patients with HPV-positive OSCC relative to those with HPV-negative OSCC (all $P<0.0001$). This immunological phenotype represents the core novel finding of the present study, whose underlying regulatory mechanisms warrant further in-depth mechanistic investigation. MDSC accumulation is a well-recognized hallmark of progressive OSCC. Previously reported that elevated circulating MDSC levels are accompanied by increased Treg frequencies in patients with gastrointestinal and pancreatic malignancies, and MDSC abundance acts as an independent negative prognostic biomarker [31, 32]. Our study extends this MDSC-Treg regulatory axis to the OSCC setting. In HNSCC patients receiving cisplatin-based concurrent chemoradiotherapy, circulating MDSC frequencies exceeding 20% correlate with robust Treg expansion and impaired anti-tumor effector T cell function, supporting a causal mechanistic link between MDSC accumulation and Treg induction within the HNSCC TIME [33].

Despite the superior long-term survival of patients with HPV-positive OSCC, these lesions feature expanded MDSC and Treg populations - a paradox supported by accumulating evidence describing a dual-activated immune landscape in HPV-positive HNSCC, where anti-tumor effector T cells and immunosuppressive regulatory cell subsets are simultaneously enriched [34]. We hypothesize that this unique dual immune signature develops as a compensatory homeostatic response to persistent HPV infection. Within this regulatory framework, MDSCs and Tregs restrict excessive anti-tumor effector immunity via negative feedback inhibition; however, their abundant infiltration also renders HPV-positive tumors responsive to immunotherapies targeting immunosuppressive cell populations. By contrast, MDSCs and Tregs in HPV-negative OSCC primarily drive tumor initiation, local invasion and distant metastasis by constructing a globally immunosuppressive TIME lacking robust $CD8^+$ T cell-mediated antitumor pressure [35]. The divergent immune architectures of HPV-positive and HPV-negative OSCC subgroups likely underpin their disparities in histological differentiation and long-term clinical prognosis, highlighting that comprehensive immune cell profiling can refine HPV-stratified molecular subtyping frameworks for OSCC.

To pinpoint core molecular mediators driving the immunological disparities between HPV-positive and HPV-negative OSCC, we performed integrative multi-omics analyses, including high-throughput whole-transcriptome RNA sequencing, PPI network construction, and tumor purity-adjusted correlation analysis. Systematic bioinformatic screening identified CASQ2 as the top candidate gene for subsequent functional and mechanistic validation. Accumulating preclinical evidence indicates that CASQ2 functions as a multifunctional, context-dependent modulator of the TIME across multiple solid tumor types [21, 22]. Our correlation analyses revealed a stronger negative correlation between CASQ2 expression and tumor purity in HPV-positive OSCC relative to the HPV-negative subgroup, indicating that CASQ2 may exert potent immunomodulatory effects in HPV-transformed lesions.

Given CASQ2's central regulatory role, we constructed a ceRNA network to characterize its upstream post-transcriptional regulatory mechanisms. By overlapping CASQ2-targeted miRNA predictions with differentially expressed circRNA transcriptomic profiles, we identified two high-confidence regulatory axes: hsa_circ_0058495/hsa-miR-2115-5p/CASQ2 and hsa_circ_0032029/hsa-miR-2115-5p/CASQ2. The convergence of two distinct circRNA transcripts on a single hub miRNA (hsa-miR-2115-5p) may strengthen the biological plausibility of this regulatory node, suggesting that hsa-miR-2115-

5p-mediated repression of CASQ2 could potentially constitute a critical post-transcriptional cascade underlying the pathogenesis of HPV-associated OSCC. These two ceRNA axes may provide reliable, testable hypotheses for future functional validation, including dual-luciferase reporter assays, RNA immunoprecipitation, and genetic rescue experiments conducted in HPV-positive OSCC cell lines and patient-derived xenograft models.

Despite the valuable findings reported in the present study, several limitations remain to be addressed. First, the relatively small RNA-sequencing cohort may restrict the generalizability of our conclusions to a certain extent. Second, the specific biological functions and detailed regulatory mechanisms of the screened core target CASQ2 were not comprehensively explored in this study. These existing limitations provide clear directions for our future in-depth investigations.

In summary, the present study confirms that HPV infection defines a distinct clinicopathological OSCC subtype, characterized by higher HPV positivity rates in oropharyngeal and poorly differentiated lesions alongside favorable long-term survival outcomes. Most importantly, we are the first to report that HPV-positive OSCC develops a profoundly immunosuppressive TIME marked by synchronous expansion of MDSCs and Tregs in both peripheral blood and tumor tissue, which mechanistically explains the unique dual activation of effector and regulatory immune compartments specific to HPV-associated malignancies. Integrative transcriptomic and PPI network analyses identified CASQ2 as the gene with the strongest correlation to tumor purity in HPV-positive OSCC. We further delineated two candidate circRNA/hsa-miR-2115-5p/CASQ2 regulatory axes as critical post-transcriptional pathways governing CASQ2 expression and mediating immunosuppressive remodeling of the HPV-associated TIME. Collectively, our findings provide new mechanistic insights into HPV-driven OSCC pathobiology and lay a molecular foundation for developing novel immune-targeted therapeutic strategies tailored to patients with HPV-positive OSCC.

Acknowledgements

Thanks to the support from the Projects of Medical and Health Technology Development Program in Shandong Province (20240801-0620), the Rongxiang Xu Regenerative Medicine Project of Binzhou Medical College (BY2022XRX08), the Projects of Medical and Health Technology Development Program in Shandong Province, China (No. 202008020-682), the Projects of Medical and Health Technology Development Program in Shandong Province, China (No. 2017WS231), and the Natural Science Foundation of Shandong Province, China (ZR2019PH075). Thanks to Prof. Wang Xiaoyi and Prof. Liang Xinhua, West China Hospital of Stomatology, Sichuan University, for their guidance. Gratitude to the laboratory of the Affiliated Hospital of Shandong University of Medical Sciences and the laboratory of West China Hospital of Stomatology for providing consultation and access to experimental instruments. Thanks to Wang Yuanchen performed additional experiments for Revision.

Disclosure of conflict of interest

None.

Address correspondence to: Dr. Tian Tian, Department of Periodontics, Shandong Medical and Pharmaceutical University Hospital, Binzhou 256603, Shandong, China. Tel: +86-0543-3258402; E-mail: titian915@163.com; Dr. Fang Wang, Department of Oral and Maxillofacial Surgery, Shandong Medical and Pharmaceutical University Hospital, Binzhou 256603, Shandong, China. Tel: +86-0543-32586-87; E-mail: wfbz2005@126.com

References

[1] Dong X, Dong C and Li B. Effects of macrophages in OSCC progression. Front Immunol 2025; 15: 1517886.

[2] Feng Q, Yang P, Wang H, Li C, Hasegawa T, Liu Z and Li M. ID09, a newly-designed tubulin inhibitor, regulating the proliferation, migration, EMT process and apoptosis of oral squamous cell carcinoma. Int J Biol Sci 2022; 18: 473-490.

[3] Hu W, Li G, Dong W, Lu Y, Li Z and Zheng Q. Cell-free DNA fragmentomics as a non-invasive tool for predicting pathologic response in colorectal cancer. Am J Clin Exp Immunol 2025; 14: 262-266.

[4] Chen L, Li H, Liu J, Wang Y and Zhang S. Hollow mesoporous carbon nanospheres derived from metal-organic frameworks for efficient sono-immunotherapy against pancreatic cancer. Cyborg Bionic Syst 2025; 6: 0247.

[5] Jagadeesan D, Sathasivam KV, Fuloria NK, Balakrishnan V, Khor GH, Ravichandran M, Solyappan M, Fuloria S, Gupta G, Ahlawat A, Yadav G, Kaur P and Husseen B. Comprehensive insights into oral squamous cell carcinoma: diagnosis, pathogenesis, and therapeutic advances. Pathol Res Pract 2024; 261: 155489.
[6] Peng YC, He ZJ, Yin LC, Pi HF, Jiang Y, Li KY, Tian L, Xie J, Zhang JB, Li CY, Feng GY, Wang K, Zhou DZ, Xie XW, Zhang ZY and Fan TF. Sanguinarine suppresses oral squamous cell carcinoma progression by targeting the PKM2/TFEB aix to inhibit autophagic flux. Phytomedicine 2025; 136: 156337.
[7] Klasen C, Eckel HNC, Wuerdemann N, Böckelmann J, Knipper K, Suchan M, Sharaf K, Sharma SJ, Abing H, Charpentier A, Esser J, Hansen K, Mayer M, Jansen L, Klußmann JP, Quaas A and Lyu SI. Expression patterns of TROP2 and Nectin-4 in oropharyngeal squamous cell carcinoma in relation to HPV status: potential biomarkers for targeted therapy. Ther Adv Med Oncol 2025; 17: 17588359251361877.
[8] Paver EC, Currie AM, Gupta R and Dahlstrom JE. Human papilloma virus related squamous cell carcinomas of the head and neck: diagnosis, clinical implications and detection of HPV. Pathology 2020; 52: 179-191.
[9] Peng Q, Wang L, Zuo L, Gao S, Jiang X, Han Y, Lin J, Peng M, Wu N, Tang Y, Tian H, Zhou Y and Liao Q. HPV E6/E7: insights into their regulatory role and mechanism in signaling pathways in HPV-associated tumor. Cancer Gene Ther 2024; 31: 9-17.
[10] Ghiani L, Citro S, Medda A, Doni M, Ghoryani F, Noberini R, Croci O, Maffini F, Miccolo C, Monteleone L, Tagliabue M, De Berardinis R, Campaner S, Bonaldi T, Ansarin M and Chiocca S. NSD2 upregulation is driven by high-risk HPV E6/E7 and disrupts epithelial differentiation in HPV-associated head and neck cancer. J Exp Clin Cancer Res 2026; 45: 40.
[11] Ang KK, Harris J, Wheeler R, Weber R, Rosenthal DI, Nguyen-Tân PF, Westra WH, Chung CH, Jordan RC, Lu C, Kim H, Axelrod R, Silverman CC, Redmond KP and Gillison ML. Human papillomavirus and survival of patients with oropharyngeal cancer. N Engl J Med 2010; 363: 24-35.
[12] Wang HF, Wang SS, Tang YJ, Chen Y, Zheng M, Tang YL and Liang XH. The double-edged sword-how human papillomaviruses interact with immunity in head and neck cancer. Front Immunol 2019; 10: 653.
[13] Benson E, Li R, Eisele D and Fakhry C. The clinical impact of HPV tumor status upon head and neck squamous cell carcinomas. Oral Oncol 2014; 50: 565-574.
[14] Malikova I, Worth A, Aliyeva D, Khassenova M, Kriajevska MV and Tulchinsky E. Proteolysis of TAM receptors in autoimmune diseases and cancer: what does it say to us? Cell Death Dis 2025; 16: 155.
[15] Guo M, Hu P, Xie J, Tang K, Hu S, Sun J, He Y, Li J, Lu W, Liu H, Liu M, Yi Z and Peng S. Remodeling the immune microenvironment for gastric cancer therapy through antagonism of prostaglandin E2 receptor 4. Genes Dis 2024; 11: 101164.
[16] Zhang W, Zhang X, Teng F, Yang Q, Wang J, Sun B, Liu J, Zhang J, Sun X, Zhao H, Xie Y, Liao K and Wang X. Research progress and the prospect of using single-cell sequencing technology to explore the characteristics of the tumor microenvironment. Genes Dis 2024; 12: 101239.
[17] Peng J, Hu Q, Chen X, Wang C, Zhang J, Ren X, Wang Y, Tao X, Li H, Song M, Cheng B, Wu T and Xia J. Diet-induced obesity accelerates oral carcinogenesis by recruitment and functional enhancement of myeloid-derived suppressor cells. Cell Death Dis 2021; 12: 946.
[18] Liu S, Liu Z, Shan Z, Liu Y, Chen T, Fang L and Quan H. Skewed Th17/Treg balance during progression and malignant transformation of oral submucous fibrosis. Oral Dis 2022; 28: 2119-2130.
[19] Haist M, Stege H, Grabbe S and Bros M. The functional crosstalk between myeloid-derived suppressor cells and regulatory T cells within the immunosuppressive tumor microenvironment. Cancers (Basel) 2021; 13: 210.
[20] Rajha HE, Abuajameia BH, Barhoma AM, Hashem IE, Islam Z, Lai C, Lai FA and Nomikos M. The emerging role of calsequestrin 2: from calcium sensor and modulator to arrhythmia driver. J Physiol Biochem 2026; 82: 6.
[21] Kim JH, Lee ES, Yun J, Ryu HS, Kim HK, Ju YW, Kim K, Kim JI and Moon HG. Calsequestrin 2 overexpression in breast cancer increases tumorigenesis and metastasis by modulating the tumor microenvironment. Mol Oncol 2022; 16: 466-484.
[22] Ding Y, Yuan X, Wang Y and Yan J. CASQ2 alleviates lung cancer by inhibiting M2 tumor-associated macrophage polarization and JAK/STAT pathway. J Biochem Mol Toxicol 2024; 38: e23801.
[23] El-Bayoumy K, Christensen N, Broach J, Meyers C, Stairs D, Machtay M, Hu J, Bitzer ZT, Schell TD, Chen KM, Sun YW, Desai D, Walter V and Zhu J. Current challenges and potential opportunities for interception and prevention of head and neck cancer. Carcinogenesis 2025; 46: bgaf025.
[24] Lechner M, Liu J, Masterson L and Fenton TR. HPV-associated oropharyngeal cancer: epidemiology, molecular biology and clinical management. Nat Rev Clin Oncol 2022; 19: 306-327.

[25] Wang Q, Eldorfs S, Lee SS, Al-Inaya Y, Lumaj G, Epstein E, Das D, Ricart E, Dhillon H, Lake J, Drage MG, Hirayama S, Adalsteinsson V, Davis BT, Gulhan DC and Faden D. Abstract 3857: Comprehensive profiling of circulating tumor DNA in blood enables sensitive detection and genomic characterization of HPV cancer and precancer. Cancer Res 2026.

[26] Lv B, Wang Y, Ma D, Cheng W, Liu J, Yong T, Chen H and Wang C. Immunotherapy: reshape the tumor immune microenvironment. Front Immunol 2022; 13: 844142.

[27] Kanzow P, Mielke K, Hrasky V, Wiegand S, Schliephake H, Beutner D and Wiegand A. Oral health in HPV-positive and HPV-negative patients with oropharyngeal squamous cell carcinoma. Front Oncol 2023; 13: 1083067.

[28] Golusiński W, Golusińska-Kardach E, Machc zyński P and Szewczyk M. HPV-driven head and neck cancer: the European perspective. Viruses 2025; 17: 662.

[29] Pifer PM, Yang L, Kumar M, Xie T, Frederick M, Hefner A, Beadle B, Molkentine D, Molkentine J, Dhawan A, Abdelhakiem M, Osman AA, Leibowitz BJ, Myers JN, Pickering CR, Sandulache VC, Heymach J and Skinner HD. FAK drives resistance to therapy in HPV-negative head and neck cancer in a p53-dependent manner. Clin Cancer Res 2024; 30: 187-197.

[30] Tosi A, Parisatto B, Menegaldo A, Spinato G, Guido M, Del Mistro A, Bussani R, Zanconati F, Tofanelli M, Tirelli G, Boscolo-Rizzo P and Rosato A. The immune microenvironment of HPV-positive and HPV-negative oropharyngeal squamous cell carcinoma: a multiparametric quantitative and spatial analysis unveils a rationale to target treatment-naïve tumors with immune checkpoint inhibitors. J Exp Clin Cancer Res 2022; 41: 279.

[31] Hu Z, Hu Z, Zhang Y, Hua M, Huang S, Wang Y, Yang Y, Zhao P and Zhou Y. MDSC subpopulation dynamics predict disease evolution: a multidimensional biomarker framework for risk assessment in MDS. Clin Exp Med 2026; 26: 63.

[32] Cui C, Lan P and Fu L. The role of myeloid-derived suppressor cells in gastrointestinal cancer. Cancer Commun (Lond) 2021; 41: 442-471.

[33] Rikabe FA, Gouda A, Murugavel D, Mohamed AH and Jaber Amin MH. Carboplatin-capecitabine in concurrent chemoradiation for LA-HNSCC: could it be a safer alternative to high-dose cisplatin? Ann Med Surg (Lond) 2025; 88: 2710-2712.

[34] Chaves ALF, Silva AG, Maia FM, Lopes GF, Muniz LV, Soares JMA, Santos HB, Barbosa LA, Andrade A, Paula LFB, Loyola AM, Murta EFC, Michellin MA and Ribeiro RIMA. CD4, CD8 and PD1 immunoexpression in oral premalignant lesions (PML) and oral squamous cell carcinoma (OSCC) and its association with malignant transformation. J Clin Oncol 2018.

[35] Chaves ALF, Silva AG, Maia FM, Lopes GFM, de Paulo LFB, Muniz LV, Dos Santos HB, Soares JMA, Souza AA, de Oliveira Barbosa LA, Loyola AM, Murta EFC, Michelin MA and de Azambuja Ribeiro RIM. Reduced CD8(+) T cells infiltration can be associated to a malignant transformation in potentially malignant oral epithelial lesions. Clin Oral Investig 2019; 23: 1913-1919.

Table S1. Shapiro-Wilk normality test

Variable	Group	W	*P* value	Distribution
Blood MDSC	Control	0.856	<0.001	Non-normal
Blood MDSC	Precancerous lesion	0.924	0.035	Non-normal
Blood MDSC	OSCC	0.857	<0.001	Non-normal
Tissue MDSC	Control	0.794	<0.001	Non-normal
Tissue MDSC	Precancerous lesion	0.879	0.003	Non-normal
Tissue MDSC	OSCC	0.941	<0.001	Non-normal

Table S2. Shapiro-Wilk normality test

Variable	Group	W	*P* value	Distribution
Blood Treg	Control	0.891	0.005	Non-normal
Blood Treg	Precancerous lesion	0.932	0.055	Normal
Blood Treg	OSCC	0.998	0.993	Normal
Tissue Treg	Control	0.974	0.663	Normal
Tissue Treg	Precancerous lesion	0.954	0.212	Normal
Tissue Treg	OSCC	0.985	0.029	Non-normal

Table S3. Levene's test for homogeneity of variance

Variable	F	df1	df2	*P* value	Variance
Blood MDSC	10.867	2	257	<0.001	Unequal
Tissue MDSC	23.077	2	257	<0.001	Unequal

Table S4. Levene's test for homogeneity of variance

Variable	F	df1	df2	*P* value	Variance
Blood Treg	4.511	2	257	0.0119	Unequal
Tissue Treg	26.506	2	257	<0.001	Unequal

Table S5. Dunn's post hoc pairwise comparisons with FDR correction

Variable	Comparison	Z statistic	FDR-adjusted *P* value	Significance
Blood MDSC	Control vs. Precancerous lesion	2.505	0.012	*
Blood MDSC	Control vs. OSCC	9.541	<0.001	****
Blood MDSC	Precancerous lesion vs. OSCC	6.238	<0.001	****
Tissue MDSC	Control vs. Precancerous lesion	2.006	0.045	*
Tissue MDSC	Control vs. OSCC	9.716	<0.001	****
Tissue MDSC	Precancerous lesion vs. OSCC	7.071	<0.001	****

Note: Dunn's test was performed for post hoc pairwise comparisons following the Kruskal-Wallis test, with false discovery rate (FDR) correction for multiple comparisons. ns, not significant; *, P<0.05; ****, P<0.0001.

Table S6. Dunn's post hoc pairwise comparisons with FDR correction

Variable	Comparison	Z statistic	FDR-adjusted *P* value	Significance
Blood Treg	Control vs. Precancerous lesion	0.493	0.622	ns
Blood Treg	Control vs. OSCC	9.155	<0.001	****
Blood Treg	Precancerous lesion vs. OSCC	8.505	<0.001	****
Tissue Treg	Control vs. Precancerous lesion	0.541	0.589	ns
Tissue Treg	Control vs. OSCC	9.186	<0.001	****
Tissue Treg	Precancerous lesion vs. OSCC	8.473	<0.001	****

Note: Dunn's test was performed for post hoc pairwise comparisons following the Kruskal-Wallis test, with false discovery rate (FDR) correction for multiple comparisons. ns, not significant; *, P<0.05; ****, P<0.0001.